applied sciences

MDPI

Article

Influence of Demagnetization and Microstructure Non-Homogeneity on Barkhausen Noise in the High-Strength Low-Alloyed Steel 1100 MC

Martin Pitoňák [1], Nikolaj Ganev [2,*], Katarína Zgútová [1], Jiří Čapek [2], Miroslav Neslušan [3] and Karel Trojan [2]

[1] Faculty of Civil Engineering, University of Žilina, Univerzitná 1, 01026 Žilina, Slovakia; martin.pitonak@uniza.sk (M.P.); katarina.zgutova@uniza.sk (K.Z.)
[2] Faculty of Nuclear Sciences and Physical Engineering, Czech Technical University in Prague, Trojanova 13, 120 00 Praha, Czech Republic; jiri.capek@fjfi.cvut.cz (J.Č.); karel.trojan@fjfi.cvut.cz (K.T.)
[3] Faculty of Mechanical Engineering, University of Žilina, Univerzitná 1, 01026 Žilina, Slovakia; miroslav.neslusan@fstroj.uniza.sk
* Correspondence: nikolaj.ganev@fjfi.cvut.cz; Tel.: +420-778-534-842

Abstract: This study deals with two different aspects of the high-strength low-alloyed 1100 MC steel. The first is associated with the remarkable heterogeneity (linked with surface decarburization) in the surface state produced during sheet rolling with respect to the sheet width. The variable thickness surface layer exhibits a microstructure different from that of the deeper bulk. Variation in the thickness of the thermally softened near-surface region strongly affects Barkhausen noise as well. This technique can be considered a reliable tool for monitoring the aforementioned heterogeneity. It can also be reported that the opposite sides of the sheet are different with respect to the surface state, the heterogeneity distribution, and the corresponding Barkhausen noise. These aspects indicate different conditions during hot rolling followed by rapid quenching on the upper and lower rollers. Furthermore, it was found that the degree of decarburizing and the corresponding surface heterogeneity is also a function of C content, and steels with lower C content exhibit less pronounced surface heterogeneity. The second aspect is related to the remarkable asymmetry in Barkhausen noise emission with respect to two consecutive bursts. This asymmetry is due to the presence of remnant magnetization in the sheet produced during manufacturing. The remnant magnetization is coupled to the magnetic field produced by the excitation coil of the Barkhausen noise sensor and strongly contributes to the aforementioned asymmetry. The remnant magnetization attenuates the domain wall mobility, which results in weaker Barkhausen noise. Moreover, the Barkhausen noise envelopes and the extracted features such as the position of the envelope maximum and its width are strongly affected by the remnant magnetization. Insufficient demagnetization makes the body magnetically softer and makes a wider range of magnetic fields in which Barkhausen noise emission can be detected. As soon as sufficient removal of this remnant magnetization is carried out in the vanishing magnetic field (demagnetization), the aforementioned remarkable asymmetry is fully lost.

Keywords: high-strength steel; Barkhausen noise; surface heterogeneity; asymmetry

Citation: Pitoňák, M.; Ganev, N.; Zgútová, K.; Čapek, J.; Neslušan, M.; Trojan, K. Influence of Demagnetization and Microstructure Non-Homogeneity on Barkhausen Noise in the High-Strength Low-Alloyed Steel 1100 MC. *Appl. Sci.* **2024**, *14*, 1511. https://doi.org/10.3390/app14041511

Academic Editors: Cem Selcuk, Beata Białobrzeska and Robert Jasinski

Received: 21 November 2023
Revised: 30 January 2024
Accepted: 8 February 2024
Published: 13 February 2024

1. Introduction

High-strength low-alloyed steels (HSLAs) are well-known materials with a very good ratio between high yield and ultimate strength and low cost. These materials are frequently used in the automotive, petrochemical, and civil industries for heavily loaded parts [1,2]. Their application also enables a reduction in the weight of construction for improved corrosion resistance [3]. The low content of alloying elements with respect to their hardening is compensated by thermo-mechanical treatment and a small addition of Nb, Ti, and/or V. The sheets of HSLAs are usually rolled at elevated temperatures (above the austenitization temperature), followed by rapid cooling. The final strength of HSLAs is a function of hot rolling conditions and the superimposed rate of consecutive cooling [2–5]. Furthermore, Nb, Ti, and V can play a certain role in microstructure refinement, their precipitates, and dissolution in the matrix [3,5–7]. The microstructure of thermo-mechanically treated low-alloyed steels of lower strength is mostly composed of refined ferrite as soon as the refined ferrite matrix becomes a mixture of ferrite + bainite or bainite + martensite. However, increasing strength comes at the expense of reduced toughness [1,8], and the residual stresses are also altered [8].

Components and structures made of HSLAs are very often of vital importance with respect to the reliability of the system and their long-term use. Their functionality is a function of the initial state, design, load manner, etc. Their non-destructive monitoring in different applications is essential.

Magnetic Barkhausen noise (MBN) is obtained during the magnetization of ferromagnetic bodies in an altered magnetic field. Domain walls (DWs) are pinned in their positions due to the presence of lattice imperfections, and their sudden motion in the form of irreversible jumps occurs when the external magnetic field reaches the pinning strength of the pinning sites [9,10]. Electromagnetic or acoustic pulses produced by these DWs during their irreversible motion can be detected on the free surface. MBN is sensitive to the microstructure due to interference between DWs and all lattice imperfections, especially dislocation tangles [11,12], precipitates [13,14], grain boundaries [15,16], hard-ferromagnetic or/and non-ferromagnetic phases [17], etc. Furthermore, preferential crystallography and the corresponding magnetic alignment (anisotropy) affect the angular distribution of MBN [18]. Finally, certain contributions of the stress state to MBN should be considered due to the positive magnetostriction and biaxial anisotropy of Fe alloys [19,20].

Consecutive bursts of MBN are usually very similar when the surface is magnetized through the hysteresis loop. Two consecutive bursts represent the ascending and descending routes of a magnetic field. However, these bursts may be different in some cases. During hard milling, such an asymmetry can be found due to the magneto-coupling between the hard white layer and the underlying soft heat-affected zone [21]. This effect was also observed in an amorphous bilayer ribbon (Fe73.5Nb3Si13.5B9Cu1/Fe74.5Nb3Si13.5B9) consisting of two layers of different magnetic hardness [22]. Similar behavior was reported with respect to plastic deformation under the uniaxial tensile test when this asymmetry was produced as a result of heterogeneity in dislocation density among neighboring grains and the associated differences in magnetic hardness of mutually coupled grains [23].

The lack of structure homogeneity is nowadays an important aspect of component functionality, as reported in many studies. Coarse grains can result in deformation heterogeneity under some conditions [24]. In some conditions, this heterogeneity can result in premature failure [25]. However, in some cases, structural heterogeneity can improve mechanical properties, especially in additively manufactured wire arc stainless steel [26]. Furthermore, the combination of chemical and microstructural heterogeneities can result in superior strength–ductility of manganese steels [27].

MBN is sensitive to alterations in microstructure and the stress state. The preliminary inspection of the delivered sheet made of 1100 MC revealed a remarkable fluctuation in MBN along the sheet width. The non-uniform MBN emission is linked with the missing demagnetization of the sheets after thermomechanical processing as well as the superimposing contribution of microstructure heterogeneity in the near-surface region. The components made of this steel could potentially be monitored by the MBN technique with respect to their microstructure (damage developed as a result of the long-term loading) and as well as their stress state. However, the non-uniform MBN emission in different regions of the sheet makes the monitoring of these components quite a difficult task since the aforementioned aspects might alter the evolution of MBN versus the microstructure and/or stress state. For these reasons, MBN signal interpretation could be quite complicated. Therefore, this study demonstrates the significance of the demagnetization process for true and reliable MBN measurement and its influence on the evolution of MBN versus tensile stress. Furthermore, the contribution of microstructure heterogeneity and the influence of the matrix chemistry are analyzed since these aspects are vital of importance as well.

2. Materials and Methods

A diagram of consecutive steps with respect to the solved topic is depicted in Figure 1. The experiments were carried out on the HSLA 1100 MC (nominal yield strength 1100 MPa) received in the form of a sheet with a length of 3000 mm, width of 1600 mm, and thickness of 6 mm. The chemical composition of 1100 MC is indicated in Table 1. The microstructure of this steel is composed of martensite with a small fraction of bainite. The exact conditions of hot rolling, as well as the cooling rate, are not known. The bulk microstructure of this steel is depicted in Figure 2.

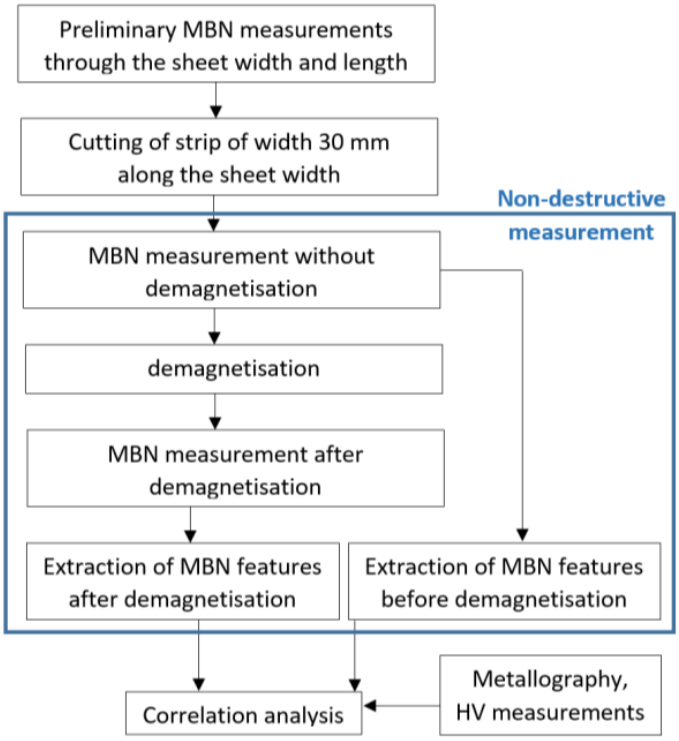

Figure 1. Brief diagram of the consecutive steps.

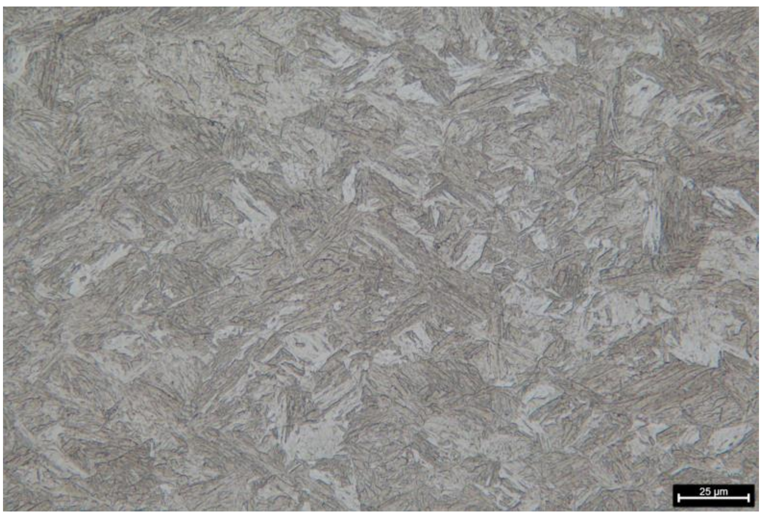

Figure 2. Bulk microstructure of HSLA 1100 MC.

Table 1. Chemical composition of 1100 MC and 1100 QL in wt.%.

	Fe	C	Mn	Si	P	Al	Nb + Ti
1100 MC	bal.	<0.15	<1.8	<0.5	<0.02	>0.015	0
1100 QL	bal.	0.08	<2.0	<0.5	<0.01	>0.060	0.02

Preliminary screening of the received sheet revealed remarkably different MBN along the sheet width, whereas a much less pronounced heterogeneity was found along the sheet length. Additionally, a difference in the MBN with respect to the different sides of the sheet was also detected. The opposite sides of the sheet were marked as side A and side B. The MBN emission was measured along the width of the sheet in step 5 mm (318 measured points) in the center of the sheet with respect to its length. The excitation field was loaded along the rolling direction (RD), which corresponds to the length of the sheet. The transversal direction is abbreviated as TD.

A strip with a width of 50 mm was cut from the as-received sheet along the sheet width. The cutting was performed in the sheet center with respect to its length. MBN measurements were performed on this strip in the as-received state in the magnetized state on sides A and B in the RD as well as the TD. The strip demagnetization was performed as a handmade operation using a Selos HD-2 (Selos, Trenčín, Slovakia) demagnetizing device in the vanishing magnetic field, and two subsequent demagnetization passes were carried out in order to avoid insufficient demagnetization. The efficiency of the demagnetization process was analyzed by the visual observation of two consecutive MBN bursts (their symmetry). MBN measurements in the demagnetized state were performed afterward on both sides in the RD and the TD.

The microstructure of the near-surface region was observed at two different positions exhibiting different MBN. Small specimens with a length of 20 mm were cut along the RD, hot molded, ground, polished, and etched by 3% Nital for 5 s. Optical images were observed on the Neophot 2 microscope with Niss Elements software 5.21.00. Thermal softening of the near-surface region was checked by microhardness measurement HV0.1 using the Innova Test 400TM (Innovatest, Maastricht, The Netherlands) device (100 g load, dwell time 10 s).

MBN was measured in the RD and the TD using the RollScan 350 (Stresstech, Jyväskylä, Finland) device coupled with the commercially available sensor S1-18-12-01 (Stresstech, Jyväskylä, Finland). The device was controlled by MicroScan500 software MicroScan500 (Stresstech, Jyväskylä, Finland) (altering the magnetic field $\pm$4.6 kA.m^{-1} at a frequency of 125 Hz, detecting a range of MBN pulses from 10 to 1000 kHz). MBN represents the *rms* (root mean square) value of the obtained MBN signal. MBN envelopes were constructed based on the filtered MBN signal, and the *PP* (Peak Position) and *FWHM* (Full Width at Half Maximum) of the MBN envelopes were analyzed as well. The *PP* is the magnetic field in which the maximum of the MBN envelope can be found. All extracted MBN features were obtained from 10 consecutive MBN bursts. Analysis of the evolution between MBN (as well as the extracted features such as *PP* and *FWHM*) and tensile stresses (in the region of elastic stresses only) was carried out under the same magnetizing conditions as listed above. Tensile stresses up to 1000 MPa were produced using an Instron 5985 (Instron, Norwood, USA) device on specimens with a length of 250 mm and a width of 22.5 mm. The MBN as well as the extracted features were measured in the RD and the TD.

Residual stresses were determined along the rolling direction (RD) and the transverse direction (TD). The XRD records were measured by a Proto iXRD Combo diffractometer with chromium radiation. The diffraction lines {*211*} were measured, and the X-ray elastic constants $½s_2$ = 5.75 TPa^{-1} and s_1 = $-$1.25 TPa^{-1} were used for the stress calculation using the software XrdWin32. The effective penetration depth of the X-ray radiation was approx. 5 μm.

In order to investigate the influence of the chemistry as well as the thermomechanical processing of the surface heterogeneity, additional high-strength low-alloyed steel was analyzed such as 1100 QL. Its chemical composition can be found in Table 1. The microstructure of 1100 QL is fully martensitic.

3. Results and Discussion

3.1. Metallographic Observations and Microhardness Measurements

Figure 3 shows the metallographic images of the surface on side A in two different positions. These positions were chosen as the locations emitting the lowest (540 mV) and highest (1440 mV) MBN after demagnetization. Figure 3a shows that the near-surface is not fully composed of martensite, but the microstructure is gently altered in the thin layer below the free surface. These laths are mixed with fine ferrite equiaxed grains, which appear white on the metallographic image. This effect becomes more pronounced in Figure 3b. This figure clearly demonstrates that the fine ferrite fully replaces the martensite in the near-surface region, and its extent is deeper in the bulk compared with Figure 3a. Figure 3b also shows that the fine ferrite is also mixed with martensite (or bainite) in the deeper regions, and the fraction of fine ferrite decreases towards the bulk at the expense of lath martensite (or bainite).

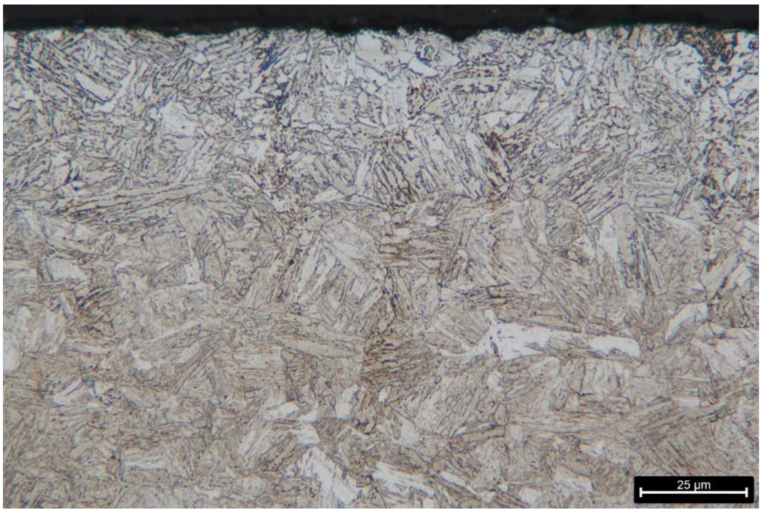

(**a**)

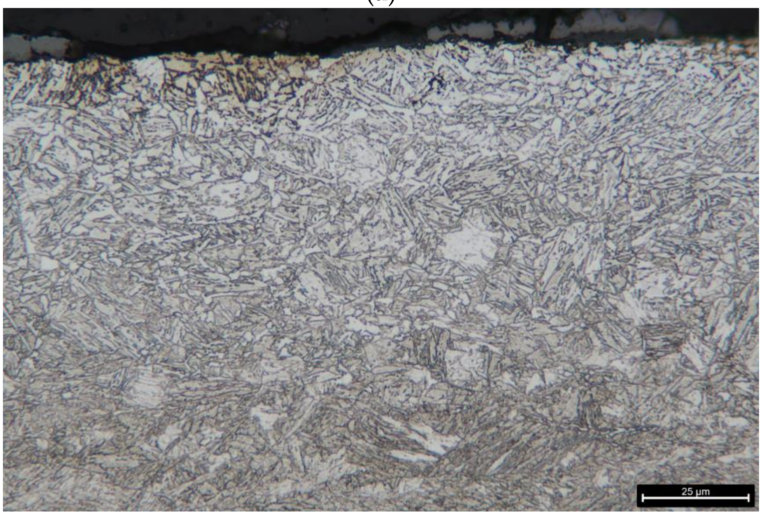

(**b**)

Figure 3. Metallographic images of the surface emitting different MBN in RD after demagnetization (1100 MC): (**a**) MBN = 540 mV and (**b**) MBN = 1440 mV.

Figure 4 indicates that the near-surface region is softened in contrast to the deeper bulk. The degree and extent of this thermal softening are deeper for the region emitting higher

MBN. Thermo-mechanically treated sheets made of 1100 MC are hot rolled at temperatures exceeding the austenitization temperature. Performing such a process in the ambient atmosphere results in near-surface decarburizing. The transformation of martensite requires very high cooling rates, as well as a sufficient C content. The transformation of martensite is the shear process due to the over-saturation of C in the Fe lattice [28]. Decarburization remarkably reduces C over-saturation, which attenuates the shear process and results in a lower dislocation density. That is the reason why the decarburized surfaces suffer from softening. The decarburized layer usually appears white on metallographic images [29,30].

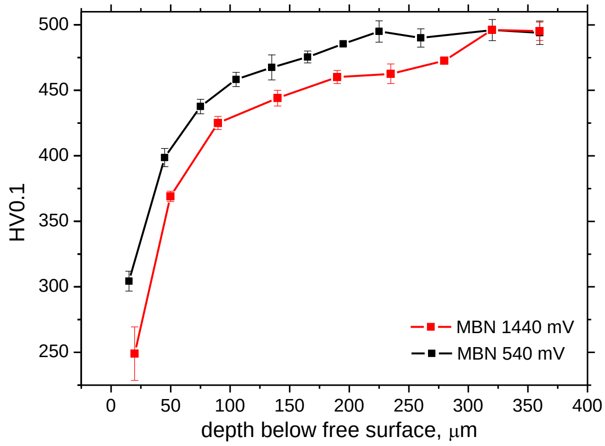

Figure 4. HV0.1 profiles for the positions emitting different MBN in the RD.

Due to the low penetration depth of decarburization and the corresponding microstructure heterogeneity, mechanical properties examined in the regions emitting different MBN (such as ultimate and yield strength as well as elongation at break) are nearly unaffected (above the nominal ones, uniaxial tensile test).

3.2. MBN Measurements

Figure 5 shows two important aspects associated with the surface and the corresponding MBN. The first is related to the valuable heterogeneity in MBN with respect to the sheet width. In particular, the regions near the sheet edge emit much higher MBN in the RD. Moreover, the opposite sites (A and B) are also different, and the MBN for side B in the RD is much higher than that for side A. The MBN in the TD is lower, and the heterogeneity in the MBN distribution is less pronounced. The remarkable heterogeneity in MBN (especially for RD) is due to the different degrees and the extent of decarburization in the different regions [31]. Higher MBN is related to more developed decarburizing, and vice versa.

The second aspect is associated with the differences between MBN before and after demagnetization; see Figures 5–7. MBN in the RD exhibits magnetized values that are significantly lower than those after demagnetization. This difference is more pronounced for the regions emitting lower MBN. Furthermore, this behavior is only minor in the TD. The physical explanation for this effect is based on the presence of remnant magnetization originating from the manufacturing process (probably the heterogeneity in plastic deformation, as previously reported [27]). The motion of DW motion in ferromagnetic bodies spreads through the matrix in the form of avalanches [32,33]. The neighboring regions (or grains) are magnetically coupled [34–36], and the change in magnetization in a certain region triggers a similar process in the neighboring ones. As soon as a certain region contains remnant magnetization, DWs in this region can be remarkably attenuated or fully hindered, being magnetically coupled to the regions containing remnant magnetization. In other words, the presence of unpinned DWs produced during manufacturing (remnant magnetization) attenuates DWs in the magnetically coupled neighboring regions.

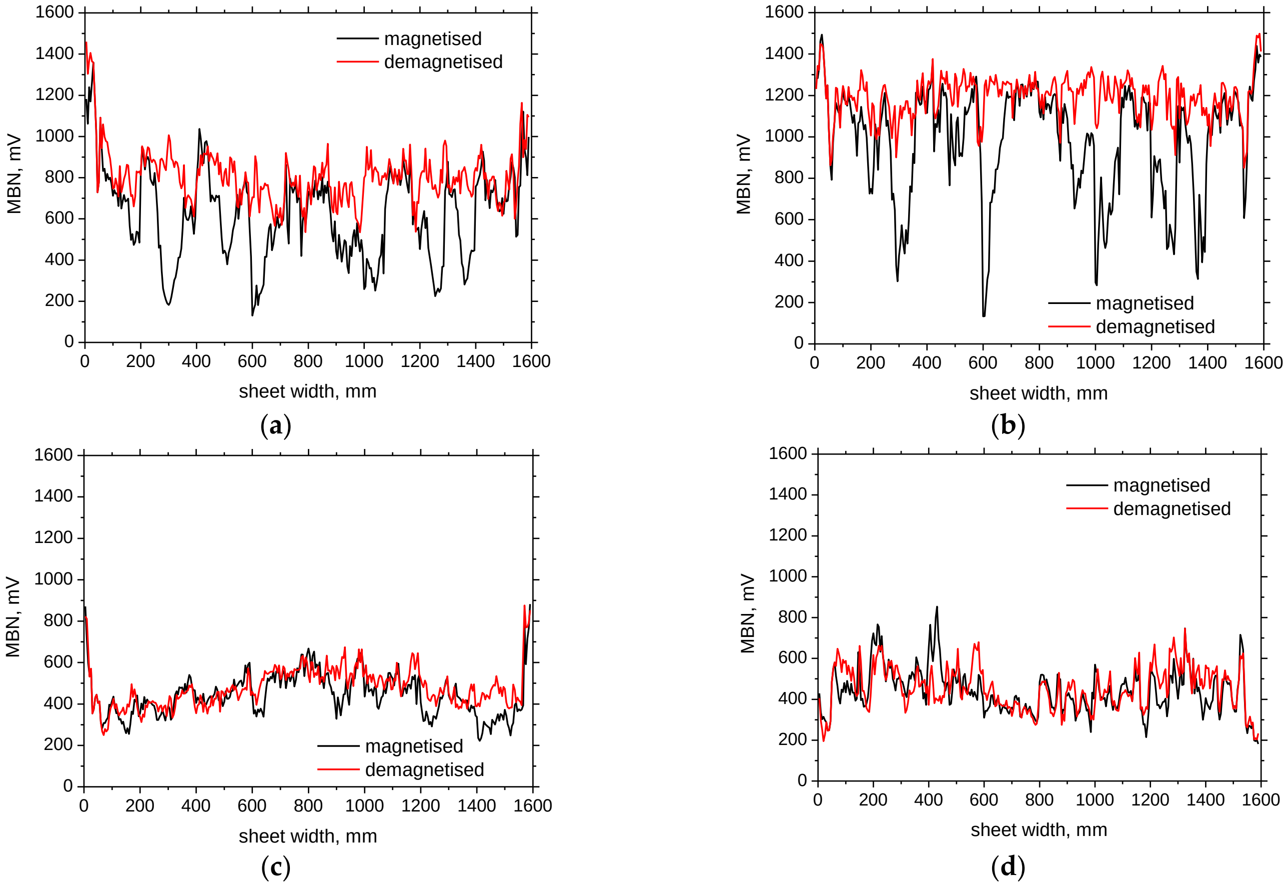

Figure 5. MBN along the sheet width; (**a**) MBN in RD—side A, (**b**) MBN in RD—side B, (**c**) MBN in TD—side A, (**d**) MBN in TD—side B.

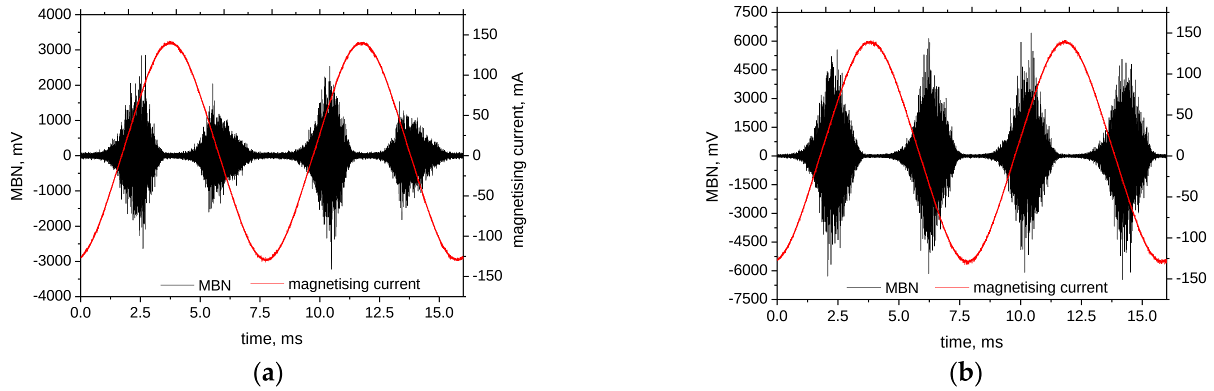

Figure 6. Four consecutive MBN bursts before and after demagnetization—side A: (**a**) before demagnetization—MBN 302 ± 32 mV and (**b**) after demagnetization—MBN 850 ± 5 mV.

Figure 5 also demonstrates the anisotropy in the remnant magnetization, since the influence of demagnetization prevails in the RD as contrasted with the TD due to the alignment of DWs in the RD. Preferential alignment of the DWs in certain directions favors the MBN in this direction and attenuates the MBN when the altered magnetic field is reversed [22]; see Figure 6 (the consecutive MBN bursts are different before demagnetization).

Apart from other aspects, MBN is also a function of DWs' speed motion v_p in m.s^{-1} (see Equation (1)).

$$v_p = \frac{dM}{dt} = (H - H_c)^q \tag{1}$$

where M is the magnetization, H is the altered magnetic field, and H_c is the magnetic field necessary for the initiation of DW motion (exponent q is about ≈ 0.5) [10,37]. Due to the presence of remnant DW alignment, H_c in the direction of DW alignment will be less compared with the reversed field, which in turn results in a different MBN. Furthermore, very high STDV (standard deviation) and asymmetry can be found in consecutive MBN bursts; see Figure 6.

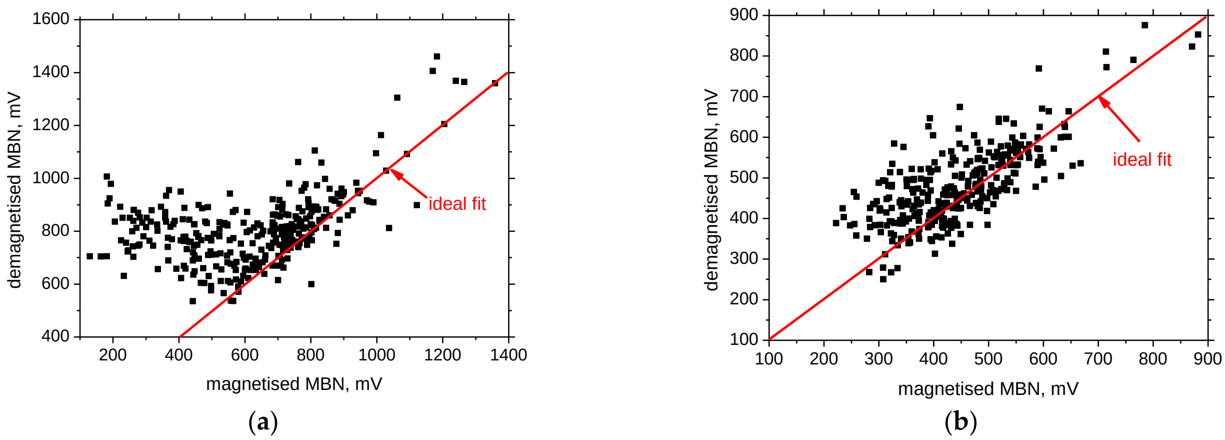

Figure 7. MBN after demagnetization versus MBN before demagnetization: (**a**) MBN in the RD—side A and (**b**) MBN in the TD—side A.

The influence of demagnetization on MBN is more pronounced in the regions emitting lower MBN after demagnetization; see Figure 7 as well as Supplementary Materials. These regions are mostly related to the less developed decarburizing and the harder matrix in terms of its mechanical and corresponding magnetic hardness. The *PP* and MBN are very often closely related when a high MBN is related to a low *PP*, and vice versa [11,38]. The magnetic field necessary to unpin DWs in regions of higher dislocation density is usually higher due to the stronger opposition of dislocation tangles to irreversible DW motion [11]. The weaker magnetic field is capable of removing the remnant magnetization in the magnetically softer regions and suppresses the influence of the demagnetization process on MBN in contrast with regions that are harder. This is because the lower influence of demagnetization of MBN and the extracted MBN features can be found near the sheet edges.

Figure 8 demonstrates that the aforementioned magnetic coupling and the presence of remnant magnetization in the sheet also affect the asymmetry of the MBN envelopes and the corresponding heterogeneity in the *PP* along with the sheet width. The presence of remnant magnetization makes the region magnetically softer, in contrast with the demagnetized state; see Figure 8. This effect is more developed in the RD, while the TD is nearly unaffected; see Figure 9.

The remarkable asymmetry in the consecutive MBN bursts before demagnetization (see Figure 6) can be directly linked to the strong asymmetry in the MBN envelopes along the descending magnetic field (negative) and the ascending one (positive); see Figure 10. Demagnetization of the sample, which completely removes the remnant magnetization, makes the MBN envelopes nearly the same with no sensitivity to the direction of the altering field. It should also be noted that the *PP* suffers from the presence of remnant magnetization, most of all MBN features. The extremely high STDV of the *PP* discriminates this MBN characteristic with respect to its use for the monitoring of the surface state and/or stress state in real applications when the component is not sufficiently demagnetized (see also Supplementary Materials).

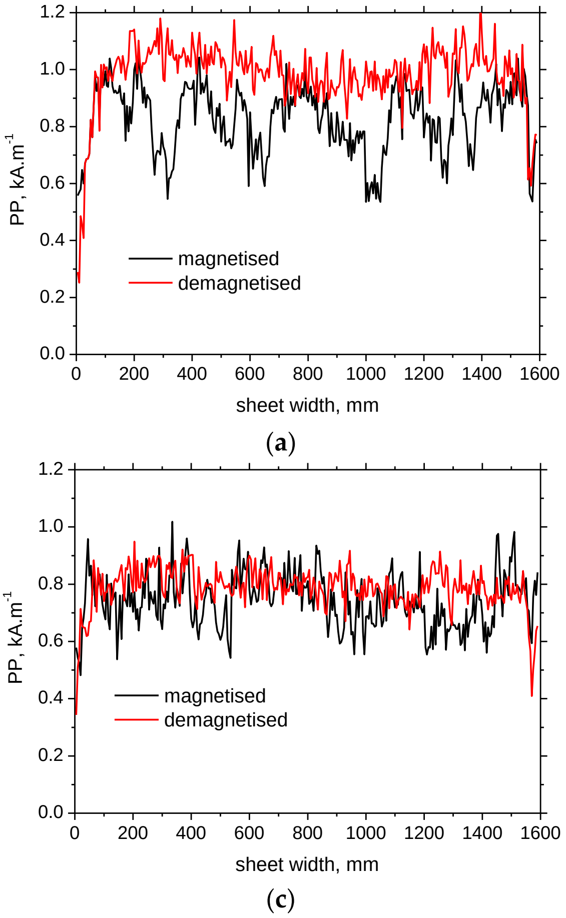

Figure 8. *PP* along the sheet width: (**a**) *PP* in the RD—side A, (**b**) *PP* in the RD—side B; (**c**) *PP* in the TD—side A; and (**d**) *PP* in the TD—side B.

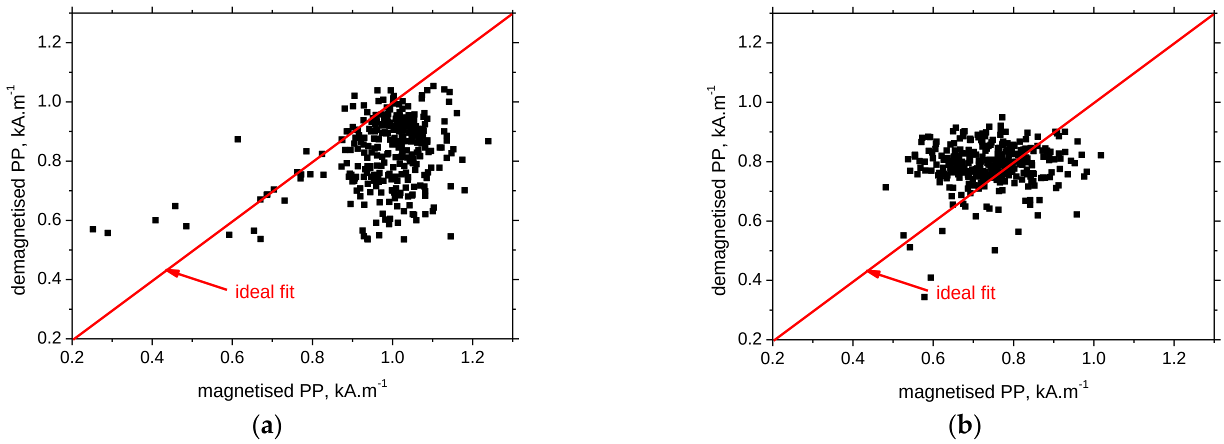

Figure 9. *PP* after demagnetization versus *PP* before demagnetization: (**a**) *PP* in the RD—side A and (**b**) *PP* in the TD—side A.

The *FWHM* is the MBN feature linked to the range of magnetic fields in which MBN emission can be detected. This parameter is also quite sensitive to the exerted stress [39]. When the preferential orientation of the matrix is developed, the conditions for the initiation of DWs in different regions (layers, grains) are very similar, MBN bursts are very narrow, and *FWHM* is low [40]. The 1100 MC MBN bursts and the corresponding *FWHM* are typical for soft magnetic bodies when MBN occurs in quite a wide range of altered magnetic fields.

Moreover, due to the superimposed magnetization of the remnant with the altered external field, the *FWHM* is higher (see Figure 11) since the conditions for unpinning DWs are very heterogeneous and directionally sensitive. The directional sensitivity can be proved by the higher differences between the *FWHM* before and after demagnetization along with the sheet width in the RD and the TD; see Figures 11 and 12.

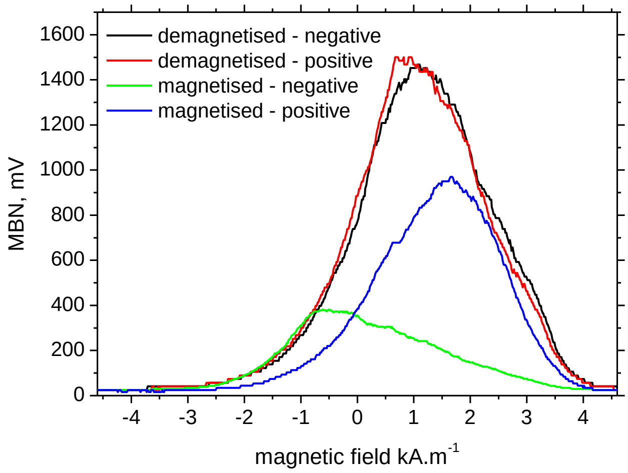

Figure 10. MBN envelopes before and after demagnetization; before demagnetization MBN 302 ± 32 mV and after demagnetization MBN 850 ± 5 mV.

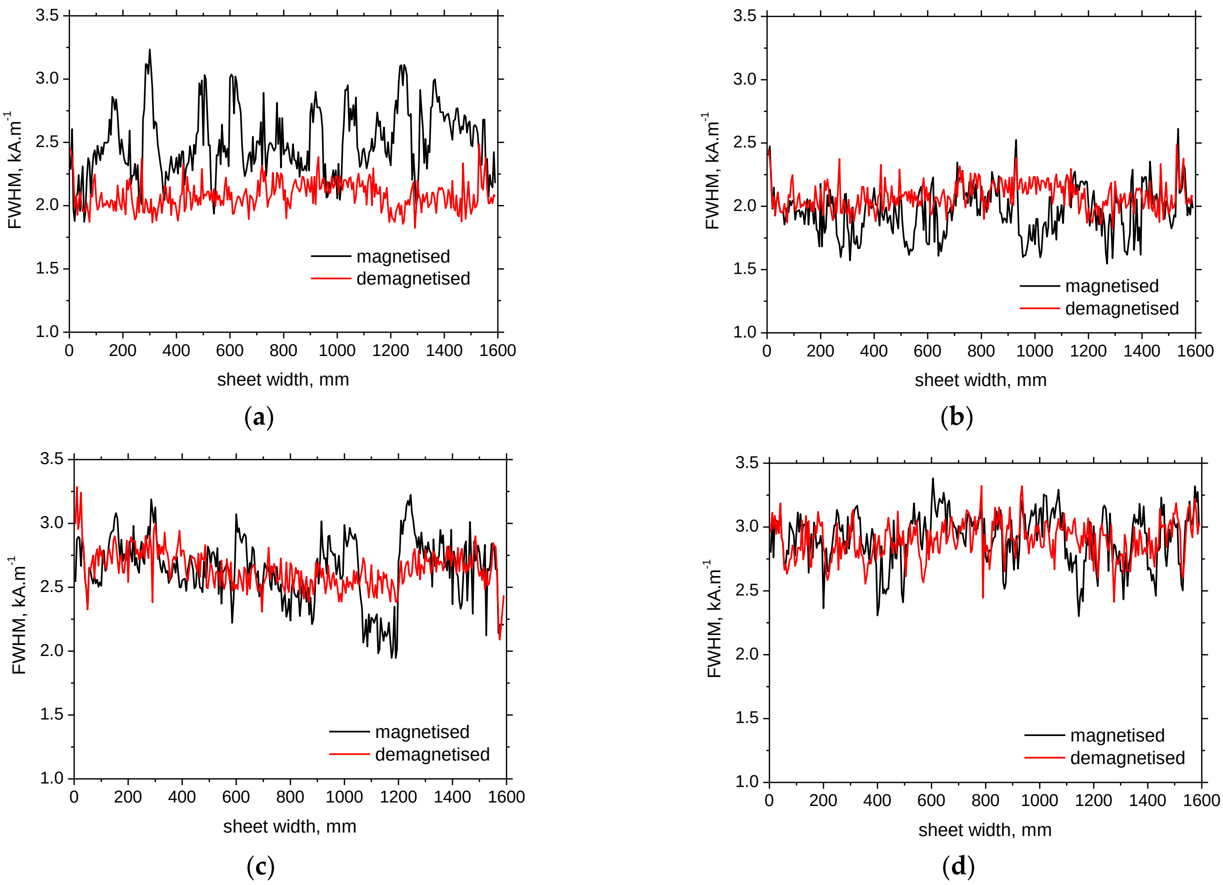

Figure 11. *FWHM* along the sheet width: (**a**) *FWHM* in the RD—side A, (**b**) *FWHM* in RD—side B, (**c**) *FWHM* in TD—side A, (**d**) *FWHM* in TD—side B.

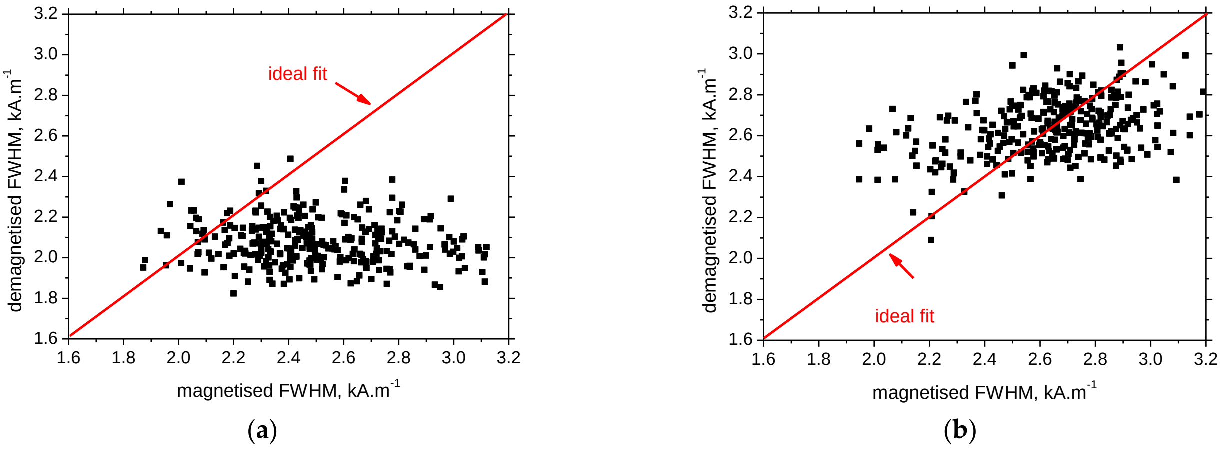

Figure 12. *FWHM* after demagnetization versus *FWHM* before demagnetization: (**a**) *FWHM* in the RD—side A and (**b**) *FWHM* in the TD—side A.

Requirements considering sufficient demagnetization are associated with the magnetic field produced by the used sensor. These fields are too weak for unpinning DWs in all regions that contribute to MBN. The situation is briefly depicted in Figure 13. Figure 13a depicts the initial state without altering the external magnetic field and with the remnant magnetization coupled to the blue region of the opposite magnetization of that in the red region. When the altered magnetizing field is strong enough, all regions can be magnetized in the direction of this field (magnetizing field highlighted by the yellow arrows); see Figure 13b,c. As soon as the magnetizing field falls below the critical threshold, the full DW alignment can be found only in the direction of the remnant magnetization; see Figure 13d. On the other hand, the effect of magnetic coupling prevails when the magnetic field is in the opposite direction to the remnant magnetization. The blue region does not contribute to the magnetization process in such case and MBN is lower in the magnetized state; see Figure 13e.

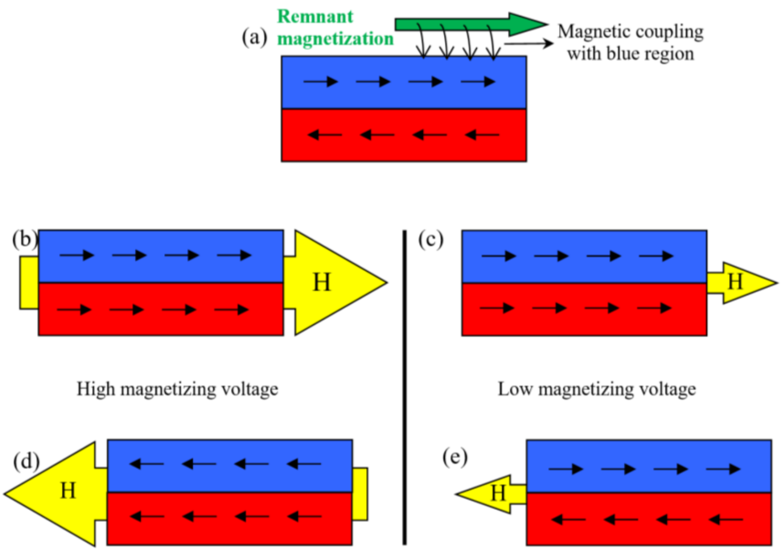

Figure 13. Magnetization process as a function of magnetizing field strength as well as remnant magnetization orientation: (**a**) the direction of remnant magnetization in demagnetized state, (**b**) magnetization in the direction of remnant magnetization at high voltage, (**c**) magnetization in the direction of remnant magnetization at low voltage, (**d**) magnetization in the opposite direction with respect of remnant magnetization at high voltage, (**e**) magnetization in the opposite direction with respect of remnant magnetization at low voltage.

Therefore, preliminary demagnetization in much stronger magnetic fields (vanishing in strength) should be carried out before MBN measurements. On the one hand, the used sensor is capable of producing a stronger magnetic field altering in time [41], which might suppress the asymmetry in consecutive MBN bursts. However, the application of such magnetizing conditions can also result in a weaker sensitivity of MBN measurements to microstructure alterations and/or stress state, as reported in, e.g., [42–44].

Finally, a brief explanation of the heterogeneity in MBN along the sheet width should be noted. MBN fluctuates in the range from 540 to 1440 mV. Such significant non-homogeneity in MBN can be addressed in different ways. The first one is based on the residual stress state, the second one is based on the microstructure alterations expressed in a variety of related aspects, and finally, the superimposing consideration of both might be considered as well. It was observed that the bulk residual stress is close to zero. The compressive stresses of magnitude of about −150 MPa can be found for the positions of MBN 540 mV for the RD. This stress is released at an early 10 µm below the free surface and reaches the bulk value. The magnitude of these compressive stresses drops down along with the increasing MBN and also releases early. The evolution of residual stresses in the TD is very similar; only the compressive stresses are about 100 MPa higher. Despite the low magnetostriction of steel, a certain contribution of decreasing stresses with respect to the increasing MBN can be considered.

However, it is considered that the main role in increasing the level of MBN should be related to the altered microstructure. Two basic aspects are detected. The first one is linked to the decreasing dislocation opposition in the near-surface region along with the increasing MBN as a result of surface decarburization. The HV0.1 15 µm below the surface was measured to be 304 $\pm$ 8 for MBN 540 mV in contrast to the bulk HV0.1 496 $\pm$ 6. The surface softening progressively vanishes towards the depth, and the affected depth is about 200 µm. However, this softening is more developed (expressed in terms of HV0.1 and its depth extent), along with the increasing MBN, and HV0.1 for MBN 1440 mV is 249 $\pm$ 12 (the affected depth is approximately 100 µm deeper in contrast to the position in which MBN is 540 mV). Finally, it should also be mentioned that MBN is also driven by the presence of very fine carbides produced during rapid cooling [3–5]. These carbides are missing in the near-surface region in comparison to the unaffected bulk. Again, the depth of the region in which missing carbides can be observed is greater for the positions of higher MBN.

The significance of these precipitates is demonstrated in Figure 14. The difference between MBN in the demagnetized and magnetized states is only minor when the surface is free of these fine carbides (as indicated by the evolution of the black and red evolutions in Figure 14). DWs can move easily, the pinning strength of the matrix is low, and the effect of the magnetic coupling due to the presence of the remnant magnetization is only minor. As soon as the decarburized layer becomes thinner and the region with fine carbides prevails within the MBN sensing depth, the effect of the remnant magnetization is mixed with the hindering effect of carbides, and the valuable difference in MBN evolution between the magnetized and demagnetized states can be found for the lower magnetizing voltages. Expressed in other words, the weaker magnetizing field is not able to overcome the remnant magnetization, and the superimposing contribution of the pinning sites is expressed in terms of fine carbides. Moreover, it can also be noted that the evolutions for the regions emitting higher MBN saturate earlier (at the lower magnetizing field linked to the magnetizing voltages), and the saturated values are remarkably higher than those for the regions emitting lower MBN due to the different contribution of carbides within the MBN sensing depth (the estimated sensing depth is about 0.1 mm in this particular case [45]).

The aforementioned topic is closely related to the components used in the automotive, petrochemical, and/or civil industries. Compositional heterogeneity, especially in multiphase steels [46] or complex phase steels [47], might be detected. In addition, the heterogeneity in the dual-phase steel structure [48] used, especially in the automotive industry or maraging steels [49], can potentially be optimized using magnetic testing.

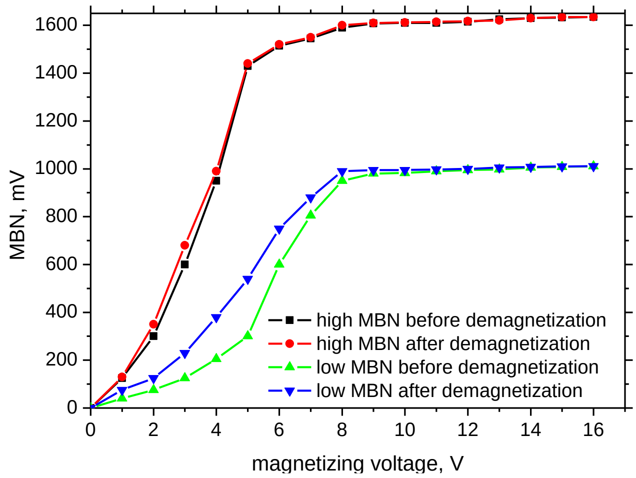

Figure 14. MBN versus magnetization voltage in the RD for the regions of high as well as low MBN before and after demagnetization.

3.3. MBN versus Tensile Stresses

The determination of the stress state on the real components is a significant task of the MBN technique. Figure 15 depicts that the remnant magnetization value affects the obtained amplitude of the stress and also affects the sensitivity of this technique expressed in terms of standard deviations, which are remarkably higher for the magnetized state. Figure 15 clearly demonstrates that the influence of the remnant magnetization on the evolution of MBN versus tensile stress is nearly none for the regions emitting high MBN. On the other hand, the regions of lower MBN exhibit remarkably lower MBN in the magnetized state, and the whole evolution is shifted to the lower MBN values. Furthermore, it should be noted that the evolutions in Figure 15 are very different, especially at the lower tensile stresses. The regions of high MBN exhibit an initial decreasing tendency, which indicates that the matrix and the corresponding DWs within the MBN sensing depth are preferentially orientated in the RD. For this reason, the energy of magneto-crystalline anisotropy is low, and the magneto-elastic energy dominates. This evolution as well as the balance between the aforementioned energies are reversed in the regions emitting low MBN, and MBN grows along with the tensile stress. The saturation phase indicates that the prevailing energies at the lower stresses are fully consumed, and the sensitivity of MBN to the tensile stress is fully lost. The evolutions of MBN in the TD exhibit much lower standard deviations in the magnetized state, and the evolutions for the demagnetized and magnetized states are closer in comparison with those in the RD (see also Supplementary Materials).

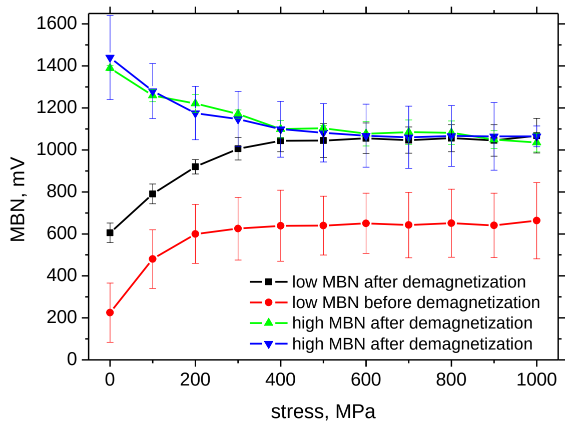

Figure 15. MBN versus tensile stress in the RD for the regions of high as well as low MBN before and after demagnetization.

3.4. Influence of Thermomechanical Treatment and Matrix Chemistry

Surface heterogeneity in low-alloyed high-strength steels with respect to MBN and the corresponding decarburization is a function of two different aspects. The first one is linked with the duration of the high-temperature cycle during hot rolling. The second one is associated with the chemical composition, especially the C content in the matrix. Figure 16 clearly depicts that the degree of surface heterogeneity for 1100 QL (expressed in MBN and PP values) is much less pronounced than that for 1100 MC (see Figure 5).

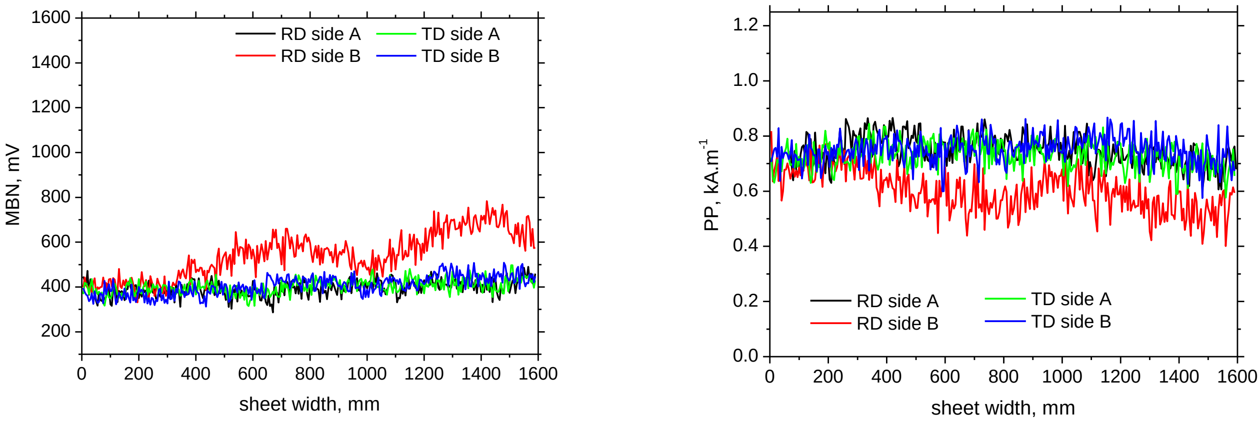

(**a**) (**b**)

Figure 16. MBN and *PP* along the sheet width for 1100 QL: (**a**) MBN QL and (**b**) *PP*.

The MC concept represents direct quenching of the sheet from the hot rolling temperatures when the final sheet thickness is obtained. The QL concept represents hot rolling followed by moderate self-cooling. The final martensite microstructure is obtained during the next heat treatment step when heating on the austenitizing temperature without rolling process assistance is followed by rapid cooling. The exact conditions with respect to hot rolling (especially the hot rolling temperature and duration of the high-temperature cycle) as well as quenching are not known (kept secret on the side of a producer). It is considered that the prolongation of high-temperature regimes results in a higher degree of surface decarburization. For this reason, the QL concept should suffer more from decarburization. However, the MBN and *PP* fluctuation range is much lower for the QL concept as contrasted against the MC concept. Also, the metallographic images depict that the near-surface microstructure alterations are less pronounced; see Figure 17. Furthermore, the *HV0.1* depth profiles demonstrate that the valuable differences in microhardness can be found in the very near surface only (about 20 µm), and *HV0.1* in the subsurface layers are quite similar; see Figure 18. Being so, it is considered that the differences in the C content play a major role. Due to the much lower C content in 1100 QL (0.08%), the diffusion rate of C is much slower than that for 1100 MC with a C content of 0.15%. Expressed in other words, the C gradient becomes steeper at elevated temperatures for the steels with higher C content, which in turn accelerates the decarburizing process.

Monitoring HSLA steels undergoing thermo-mechanical treatment using MBN is a challenging task. On the one hand, the contribution of remnant magnetization can be fully removed by sufficiently demagnetizing. This process can be quite easily checked by visual observations of consecutive MBN bursts. However, variable decarburization mixed with the components' real loading makes the application of the MBN technique for monitoring the components in use a debatable issue since the synergistic contribution of an altering microstructure and the superimposing influence of stress might be difficult to unwrap. This aspect needs further research together with deeper insight into decarburization quantification and its influence on microstructure features (the presence of fine carbides). A clear understanding of the complex behavior is vital of importance with respect to the reliable application of the MBN technique especially in the automotive and civil industries.

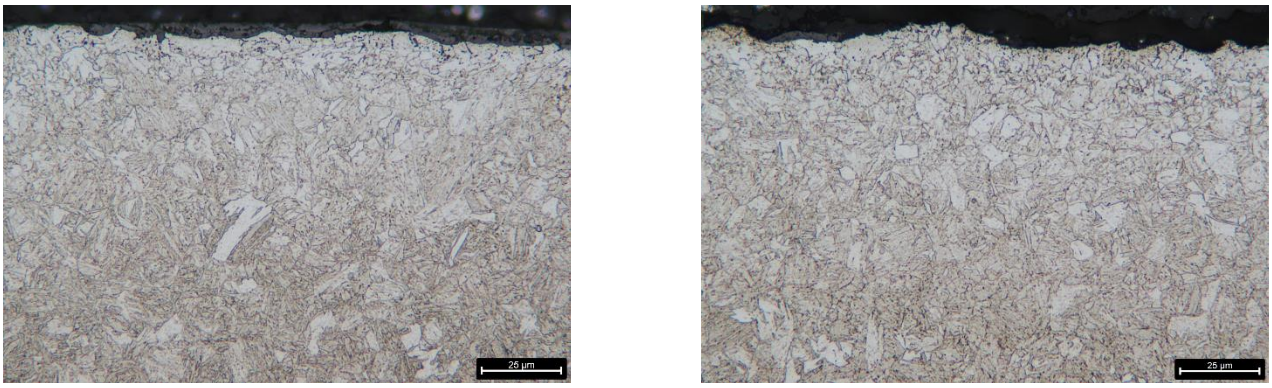

(**a**) (**b**)

Figure 17. Metallographic images of the surface emitting different MBN in the RD after demagnetization (1100 QL): (**a**) MBN = 300 mV and (**b**) MBN = 700 mV.

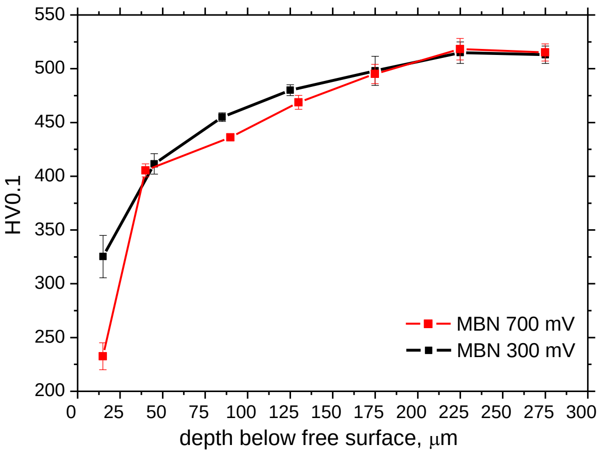

Figure 18. *HV0.1* depth profiles for 1100 QL.

4. Conclusions

The findings of this study can be summarized as follows:

- The remarkable MBN heterogeneity along with the sheet width is due to the variable decarburizing developed during hot rolling when MBN fluctuates in the range from 540 mV up to 1440 mV in the RD.
- Remnant magnetization makes the MBN heterogeneity more pronounced, and MBN (especially in the regions of lower decarburization) drops down to 150 mV.
- Also, the *PP* values fluctuate in the range from 0.3 up to 1.2 kA.m^{-1}, and this fluctuation becomes stronger in the magnetized state, whereas the fluctuation in *FWHM* is less remarkable.
- The heterogeneity in the surface state and remnant magnetization affect the evolution of MBN under the tensile stress in a synergistic manner when MBN grows in the regions of low decarburization, whereas MBN drops down in the regions with a stronger decarburizing effect (however, these evolutions saturate above 400 MPa).
- The surface heterogeneity as well as the decarburizing process become decelerated when the C content in the matrix is lower.

Supplementary Materials: The following supporting information can be downloaded at: https://www.mdpi.com/article/10.3390/app14041511/s1. Figure S1. STDV of MBN before and after demagnetization; Figure S2. STDV of PP before and after demagnetization; Figure S3. PP versus tensile stress in RD for the regions of high as well as low MBN before and after demagnetization;

Figure S4. FWHM versus tensile stress in RD for the regions of high as well as low MBN before and after demagnetization.

Author Contributions: Conceptualization, M.P., N.G. and M.N.; methodology, K.Z.; software, M.N.; validation, M.P. and N.G.; formal analysis, J.Č. and K.Z.; investigation, M.P., M.N., N.G. and K.Z.; resources, N.G.; data curation, N.G. and K.Z.; writing—original draft preparation, M.P., M.N. and N.G.; writing—review and editing, J.Č. and K.T.; visualization, J.Č. and K.T.; supervision, N.G.; project administration, M.P. and N.G.; funding acquisition, N.G. and M.N. All authors have read and agreed to the published version of the manuscript.

Funding: This work was realized within the frame of the project VEGA project 1/0052/22. This research was also supported by the Center for Advanced Applied Science, grant number CZ.02.1.01/0.0/0.0/16_019/0000778 "Center for Advanced Applied Science" within the Operational Program Research, Development and Education supervised by the Ministry of Education, Youth and Sports of the Czech Republic. This paper was also supported by the Slovak Research and Development Agency under contract No. APVV-22-0040.

Institutional Review Board Statement: Not applicable.

Informed Consent Statement: Not applicable.

Data Availability Statement: Data are contained within the article.

Conflicts of Interest: The authors declare no conflicts of interest.

References

1. Fonstein, N. *Advanced High Strength Sheet Steels*, 1st ed.; Springer International Publishing: Cham, Switzerland; Berlin, Germany, 2015. [CrossRef]
2. Ding, H.; Zhu, G.; Xiang, C.; Pei, F.; Chen, J.; Wang, Y.; Chen, Q. Excellent combination of plasticity and ultra-high strength in a low-alloy automotive steel treated by conventional continuous annealing. *Mater. Sci. Eng. A* **2020**, *791*, 139694. [CrossRef]
3. Zhang, H.K.; Xiao, H.; Fang, X.W.; Zhang, Q.; Logé, R.E.; Huang, K. A critical assessment of experimental investigation of dynamic recrystallization of metallic materials. *Mater. Des.* **2020**, *193*, 108873. [CrossRef]
4. Vervynckt, S.; Verbeken, K.; Lopez, B.; Jonas, J.J. Modern HSLA steels and role of non-recrystallisation temperature. *Int. Mater. Rew.* **2012**, *57*, 187208. [CrossRef]
5. De Ardo, A.J.; Hua, M.J.; Cho, K.G.; Garcia, G.I. On strength of micro alloyed steels: An interpretive review. *Mater. Sci. Technol.* **2009**, *25*, 1074. [CrossRef]
6. Wang, J.; Wang, S.; Xi, X.; Wang, G.; Chen, L. The role of copper in microstructure and toughness of intercritically reheated coarse grained heat affected zone in a high strength low alloy steel. *Mater. Charact.* **2021**, *181*, 111511. [CrossRef]
7. Li, S.; Yu, H.; Lu, Y.; Lu, J.; Wang, W.; Yang, S. Effects of titanium content on the impact wear properties of high-strength low-alloy steels. *Wear* **2021**, *474–475*, 203647. [CrossRef]
8. Neslušan, M.; Pitoňák, M.; Minárik, P.; Tkáč, M.; Kollár, P.; Životský, O. Influence of domain walls thickness, density and alignment on Barkhausen noise emission in low alloyed steels. *Sci. Rep.* **2023**, *13*, 5687. [CrossRef]
9. Jiles, D. *Introduction to Magnetizm and Magnetic Materials*, 3rd ed.; Taylor & Francis Group: New York, NY, USA, 2016.
10. Chikazumi, S. *Physics of Ferromagnetizm*, 2nd ed.; Oxford University Press: Oxford, UK, 2005.
11. Bayramoglu, S.; Gür, C.H.; Alexandrov, I.V.; Abramova, M.M. Characterization of ultra-fine grained steel samples produced by high pressure torsion via magnetic Barkhausen noise analysis. *Mater. Sci. Eng. A* **2010**, *527*, 927–933. [CrossRef]
12. Kleber, X.; Vincent, A. On the role of residual internal stresses and dislocations on Barkhausen noise in plastically deformed steel. *NDTE Int.* **2004**, *37*, 439–445. [CrossRef]
13. Neslušan, M.; Čížek, J.; Kolařík, K.; Minárik, P.; Čilliková, M.; Melikhová, O. Monitoring of grinding burn via Barkhausen noise emission in case-hardened steel in large-bearing production. *J. Mater. Process. Technol.* **2017**, *240*, 104–117. [CrossRef]
14. Neslušan, M.; Minárik, P.; Čilliková, M.; Kolařík, K.; Rubešová, K. Barkhausen noise emission in tool steel X210Cr12 after semi-solid processing. *Mater. Charact.* **2019**, *157*, 109891. [CrossRef]
15. Yamaura, S.; Furuya, Y.; Watanabe, T. The effect of grain boundary microstructure on Barkhausen noise in ferromagnetic materials. *Acta Mater.* **2001**, *49*, 3019–3027. [CrossRef]
16. Neslušan, M.; Minárik, P.; Grenčík, J.; Trojan, K.; Zgútová, K. Non-destructive evaluation of the railway wheel surface damage after long-term operation via Barkhausen noise technique. *Wear* **2019**, *420–421*, 195–206. [CrossRef]
17. Neslušan, M.; Bahleda, F.; Minárik, P.; Zgútová, K.; Jambor, M. Non-destructive monitoring of corrosion extent in steel rope wires via Barkhausen noise emission. *J. Magn. Magn. Mater.* **2019**, *484*, 179–187. [CrossRef]
18. Manh, T.L.; Caleyo, F.; Hallen, J.M.; Espina-Hernández, J.H.; Pérez-Benitez, J.A. Model for the correlation between magnetocrystalline energy and Barkhausen noise in ferromagnetic materials. *J. Magn. Magn. Mater.* **2018**, *454*, 155–164. [CrossRef]
19. Sorsa, A.; Santa-Aho, S.; Wartiainen, J.; Souminen, L.; Vippola, M.; Leviskä, K. Effect of shot peening parameters to residual stress profiles and Barkhausen noise. *J. Nondestruct. Eval.* **2018**, *37*, 10. [CrossRef]

20. Liu, J.; Tian, G.Y.; Gao, B.; Zeng, K.; Zheng, Y.; Chen, J. Micro-macro characteristics between domain wall motion and magnetic Barkhausen noise under tensile stress. *J. Magn. Magn. Mater.* **2020**, *493*, 165719. [CrossRef]
21. Čilliková, M.; Mičietová, A.; Čep, R.; Mičieta, B.; Neslušan, M.; Kejzlar, P. Asymmetrical Barkhausen Noise of a Hard Milled Surface. *Materials* **2021**, *14*, 1293; [CrossRef]
22. Rivas, M.; Martinéz-García, J.C.; Škorvánek, I.; Švec, P.; Gorria, P. Magnetostatic interaction in soft magnetic bilayer ribbons unambiguously identified by first-order reversal curve analysis. *Appl. Phys. Lett.* **2015**, *107*, 132240. [CrossRef]
23. Pitoňák, M.; Neslušan, M.; Minárik, P.; Čapek, J.; Zgútová, K.; Jurkovič, M.; Kalina, T. Investigation of Magnetic Anisotropy and Barkhausen Noise Asymmetry Resulting from Uniaxial Plastic Deformation of Steel S235. *Appl. Sci.* **2021**, *11*, 3600. [CrossRef]
24. Li, Y.; Shen, P.; Zhang, H.; Dong, K.; Deng, Y.; Chen, X.; Cui, Z. Deformation heterogeneity induced coarse grain refinement of the mixed-grain structure of 316LN steel through limited deformation condition. *Mater. Des.* **2021**, *210*, 110057. [CrossRef]
25. Li, W.; Li, X.; Fang, Q.; Liu, B.; Jiang, C. Plastically heterogeneity-driven fracture in additive manufactured steels. *Eng. Fract. Mech.* **2023**, *283*, 109203. [CrossRef]
26. Jafarzad-Shayan, M.M.; Zarei-Hanzaki, A.; Moshiri, A.; Seop Kim, H.; Haftlang, F.; Tahaghoghi, M.; Mahmoudi, M.; Momeni, M.; Abedi, H.R. Microstructural heterogeneity and exceptional mechanical properties in a wire-arc additively manufactured stainless steel. *Mater. Sci. Eng. A* **2023**, *882*, 145473. [CrossRef]
27. Dépinoy, S. Influence of solidification conditions on chemical heterogeneities and dislocations patterning in additively manufactured 316L stainless steel. *Materials* **2022**, *24*, 101472. [CrossRef]
28. Smallman, R.E. *Modern Physical Metallurgy*, 4th ed.; Butterworth-Heinemann: Oxford, UK, 1985. [CrossRef]
29. Kanematsu, Y.; Uehigashi, N.; Matsui, M.; Noguchi, S. Influence of a decarburized layer on the formation of microcracks in railway rails: On-site investigation and twin-disc study. *Wear* **2022**, *504–505*, 204427. [CrossRef]
30. Stupakov, O.; Perevertov, O.; Tomáš, I.; Skrbek, B. Evaluation of surface decarburization depth by magnetic Barkhausen noise technique. *J. Magn. Magn. Mater.* **2011**, *323*, 1692–1697. [CrossRef]
31. Neslušan, M. *Decarburizing of HSLA after Thermo-Mechanical Processing*; Research Report n.08/2022; University of Žilina: Žilina, Slovakia, 2022.
32. Bertotti, G.; Fiorillo, F. Bloch wall motion in Si-Fe investigated through surface e.m.f. measurements. *J. Magn. Magn. Mater.* **1984**, *41*, 303–305. [CrossRef]
33. Alessandro, B.; Beatrice, C.; Bertotti, G.; Montorsi, A. Domain wall dynamics and Barkhausen effect in metallic ferromagnetic materials. II. Experiments. *J. Appl. Phys.* **1990**, *68*, 2908. [CrossRef]
34. Bohn, F.; Durin, G.; Correa, M.A.; Machado, N.R.; Pace, R.D.; Chesman, C.; Sommer, R.L. Playing with universality classes of Barkhausen avalanches. *Sci. Rep.* **2018**, *8*, 11294. [CrossRef] [PubMed]
35. Hansen, U.B.; Syljuåsen, O.F.; Jensen, J.; Schäffer, T.K.; Andersen, C.R.; Jose, M.B.; Rodriguez-Rivera, A.; Christensen, N.B.; Lefmann, K. Magnetic Bloch oscillations and domain wall dynamics in a near-Ising ferromagnetic chain. *Nat. Commun.* **2022**, *13*, 2547. [CrossRef] [PubMed]
36. Tadić, B.; Mijatović, S.; Janićević, S.; Spasojević, D.; Rodgers, G.J. The critical Barkhausen avalanches in thin random-field ferromagnets with an open boundary. *Sci. Rep.* **2019**, *9*, 6340. [CrossRef]
37. Varga, R. *Domain Walls and Their Dynamics*, 1st ed.; Pavol Jozef Šafárik University: Košice, Slovakia, 2014.
38. Neslušan, M.; Jurkovič, M.; Kalina, T.; Pitoňák, M.; Zgútová, K. Monitoring of S235 steel over-stressing by the use of Barkhausen noise technique. *Eng. Fail. Anal.* **2020**, *117*, 104843. [CrossRef]
39. Šrámek, J.; Neslušan, M.; Bahleda, F.; Zgútová, K.; Schenk, P. Influence of sample size and magnetizing voltage on Barkhausen noise during bending and uniaxial tensile test. *Acta Phys. Pol. A* **2020**, *137*, 640–643. [CrossRef]
40. Neslušan, M.; Mičietová, A.; Hadzima, B.; Mičieta, B.; Kejzlar, P.; Čapek, J.; Uríček, J.; Pastorek, F. Barkhausen noise emission in hard-milled surfaces. *Materials* **2019**, *12*, 660. [CrossRef]
41. *MicroScan 600 Operating Instructions Manual V.5.4b (2015-0-06)*; Stresstech Group: Jyväskylä, Finland, 2015.
42. Neslušan, M.; Zgútová, K.; Pitoňák, M.; Kajánek, D. Influence of Magnetizing Conditions on Barkhausen Noise in Fe Soft Magnetic Materials after Thermo-Mechanical Treatment. *Materials* **2022**, *15*, 7239. [CrossRef]
43. Jedamski, R.; Heinzel, J.; Karpuschewski, B.; Epp, J. In-process measurement of Barkhausen noise for detection of surface integrity during grinding. *Appl. Sci.* **2022**, *12*, 4671. [CrossRef]
44. Bahleda, F.; Neslušan, M.; Pastorek, F.; Koňár, R.; Kubjatko, T. Barkhausen Noise Emission as a Function of Tensile Stress in Low-Alloyed Steels: Influence of Corrosion and Steel Strength. *Appl. Sci.* **2023**, *13*, 6574. [CrossRef]
45. Stupakov, A.; Perevertov, A.; Neslušan, M. Reading depth of the magnetic Barkhausen noise. II. Two-phase surface-treated steels. *J. Magn. Magn. Mater.* **2020**, *513*, 167239. [CrossRef]
46. Chang, Y.; Haase, C.; Szeliga, D.; Madej, L.; Hangen, U.; Pietrzyk, M.; Bleck, W. Compositional heterogeneity in multiphase steels: Characterization and influence on local properties. *Mater. Sci. Eng. A* **2021**, *827*, 142078. [CrossRef]
47. Chang, Y.; Lin, M.; Hangen, U.; Richter, S.; Haase, C.; Bleck, W. Revealing the relation between microstructural heterogeneities and local mechanical properties of complex-phase steel by correlative electron microscopy and nanoindentation characterization. *Mater. Des.* **2023**, *203*, 109620. [CrossRef]

48. Charleux, L.; Tabourot, L.; Roux, E.; Issack Farah, M.; Bizet, L. Dependency of the Young's modulus to plastic strain in DP steels: A consequence of heterogeneity? *Mater. Today Commun.* **2020**, *24*, 100972. [CrossRef]
49. Deng, F.; Yang, G.; Zhou, S.; Wu, B.; Qin, L.; Zheng, J. Effect of heat treatment on microstructural heterogeneity and mechanical properties of maraging steel fabricated by wire arc additive manufacturing using 4% nitrogen shielding gas. *Mater. Charact.* **2022**, *191*, 112160. [CrossRef]